The Phasor Gate and Harmonic Computation

Proposal for Proof-of-Concept Development

Thomas Paul Choboter
thomaschoboter@gmail.com
Computer Engineering Department, Cal Poly SLO

June 5, 2025

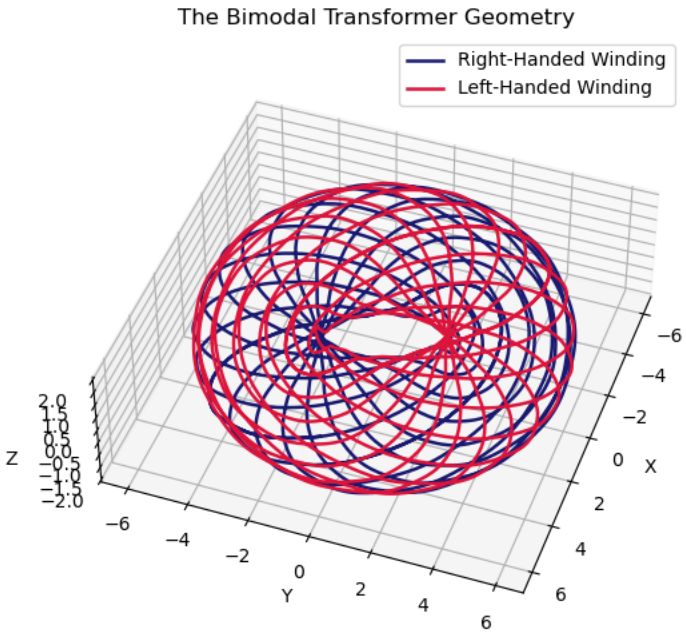

1. Introinduction

Inductors aren't just coils of wire – they are magnetic field domains in space defined by a loop of current, or a *superposition* of loops of current. For the last year, I have been exploring exotic electromagnetic field resonance geometries (LC circuits with unconventional topologies) in search of the equivalent of an 'electromagnetic gearbox' – a circuit component capable of shifting the frequency of an AC voltage input while preserving its phase information. This exploration has led to the conceptualization of the Phasor Gate, a device with the potential to redefine analog signal processing and unlock a novel computing paradigm.

Current computing technologies face fundamental limitations. Digital systems, while powerful, are hitting barriers in energy efficiency and processing speed for certain complex tasks. Quantum computing, though promising for specific problems, grapples with qubit instability, decoherence, and the probabilistic nature of measurement. There is a clear need for alternative approaches that can handle complex information robustly and efficiently. The Phasor Gate, and the Harmonic Computing paradigm it unlocks, offer such an alternative by harnessing the rich, continuous nature of analog wave phenomena in a precisely controllable way.

2. The Phasor Gate and the Bimodal Transformer

The "Phasor Gate" is a novel resonant electromagnetic device architected to perform arbitrary unitary transformations on input signals composed of superposed frequencies. At its heart lies a "bimodal transformer" featuring two counter-wound chiral (N, N-1) toroidal knot wires. This unique geometry, when coupled with a network of dynamically tunable varactors (voltage-controlled capacitors), allows for the selective excitation and manipulation of two orthogonal magnetic field modes: a Poloidal mode and a Toroidal mode. These resonance modes are important, and they are capitalized because my use of them slightly differs from convention. "Poloidal" refers to current traveling around both wires that add together constructively and destructively such that the current appears to travel around the main loop of the torus, orbiting the center. This generates the Poloidal magnetic field, which loops around the small radius of the torus, through the center, orbiting the ring. The Toroidal mode is generated by a similar constructive and destructive interference pattern, but one of the wires has the negative current of before. This makes the effective current travel as a superposition of both wires "Toroidally," around the small axis orbiting the ring, which generates a Toroidal magnetic field orbiting the center, traveling on the inside of the torus. These resonance modes are orthogonal and can therefore support any separate combination of field strengths they're rated for, by the coils' superposition of currents.

3. Varactor Configuration

Now, place two tunable capacitors of the same capacitance across both pairs of wire from one to the other. This capacitive coupling itentifies one of the modes, either Poloidal or Toroidal, in the inductor. Place two new tunable capacitors equal in capacitance to each other, but distinct from the previous two, to form a complete bipartite graph between the two terminals of one wire and the two of the other. These cross coupled capacitors identify the other mode, Toroidal or Poloidal. We now have two tunable resonance geometries that are orthogonal but can dynamically interact by shifting each mode's resonant frequency independently.

4. The Information of Superpositions

An input signal, typically a superposition of two closely-spaced frequencies (e.g., f_1, f_2), is introduced into one mode from a separate coil. By precisely controlling the varactors' capacitances via an external modulation signal (specifically, at the difference frequency $f_m = |f_1 - f_2|$ with a controllable "quasimodal phase" Θ) between the Toroidal and Poloidal varactor control waveforms, the resonant characteristics of these modes are dynamically altered. This parametric modulation facilitates coherent energy exchange and phase shifts between the f_1 and f_2 components, and their transfer to the output mode. Let's break this down.

Using this new circuit component, one can perform gate operations on "qubits" of data represented as superpositions of waveforms. A single qubit stores the equivalent of two complex values whose distances from zero, when added, equal one. This is the same as picking a value on the surface of a hypersphere with radius one. Interestingly, complex numbers are also used frequently to analyze analog circuits with alternating current and voltage waveforms. These waveforms are usually sinusoidal, and analog circuitry can already introduce phase shifts, scale amplitudes, create superpositions of frequencies, and even selectively filter a specific sinusoidal frequency to trigger events or be operated on (i.e. touch-tone telephone). The only component that's missing is phase-coherent frequency shifting, or "mode mixing". If information from one frequency can be shifted to another and retain all of its information, then each frequency in a harmonic series becomes a basis vector that can be transformed onto or combined with any other. A sinusoidal voltage waveform with a superposition of frequencies represents data with the same number of dimensions as twice the number of frequencies present (think amplitude and phase). We only need two frequencies to store the information of a single qubit.

5. Define a Reference Point

We can store the "ground" amplitude and phase for each frequency in a sawtooth wave, which is the superposition of a harmonic series with the first harmonic's period equal to the period of the sawtooth. I call this sawtooth wave the "Modal Clock," as it's first harmonic is ideal for powering the varactors at the right frequency to operate on an (N, N+1) pair of harmonics. So, not only is the modal clock able to define

phase 0 and amplitude 1 for all sinusoids in a harmonic series, in a network of Phasor Gates, it can also drive all Phasor Gates to any combination of resonant frequencies harmonic with the clock for the Poloidal and Toroidal modes, separately, and *dynamically*.

6. Pulling on Strings

The dynamic retuning of varactors is what powers a phasor gate. When energy is stored in a resonant mode of the structure, and the corresponding capacitance is changed, the resonant frequency of the field shifts but the energy inside the system remains there. It's like pulling on a guitar string after you've already played it. Repeat this detuning at the precise frequency of the modal clock, and oscillate the value of the varactors such that the resonant frequency of the corresponding T or P mode shifts between the desired operating harmonics at the extremes of its control waveform. Then, attach input and output coils. The input coil is wound exclusively around the Poloidal mode, orbiting the center of the torus, and the output coil is wound exclusively around the Toroidal mode, orbiting the ring. Surprisingly, the transfer function for this system can be rigorously described (See *Appendix B*).

7. Engineering Unitary Transformations

The interaction within the Phasor Gate can be rigorously described. The input state, represented by complex amplitudes (A_1, A_2) for frequencies f_1, f_2 in a separate input coil, is transformed into an output state (B_1, B_2) in the separate output coil. This transformation is governed by a 2×2 unitary matrix $P(\Theta, \tau)$:

$$\begin{pmatrix} B_1 \\ B_2 \end{pmatrix} = P(\Theta, \tau) \begin{pmatrix} A_1 \\ A_2 \end{pmatrix}$$

Through careful design (fixing specific operational parameters like modulation depth and interaction time τ to achieve a constant rotation angle ϕ_0), this matrix can be engineered to take the form of a rotation by ϕ_0 around an axis $\hat{n}(\Theta)$ in the X-Y plane of the analogous Bloch sphere:

$$P(\Theta) = \begin{pmatrix} \cos(\phi_0/2) & -ie^{-i\Theta}\sin(\phi_0/2) \\ -ie^{i\Theta}\sin(\phi_0/2) & \cos(\phi_0/2) \end{pmatrix}$$

Here, the quasimodal phase Θ directly controls the axis of rotation $\hat{n}(\Theta) = (\cos\Theta, \sin\Theta, 0)$. By combining this $P(\Theta)$ gate with external Z-rotations (phase adjustments to the input/output signal components), any arbitrary SU(2) unitary operation can be synthesized. This forms the basis for a universal gate. The underlying system dynamics are described by a 4×4 effective Hamiltonian for the coupled Poloidal and Toroidal mode amplitudes, the exponentiation of which yields the specific elements of $P(\Theta, \tau)$.

A full derivation of this transfer function, utilizing the Floquet method of analysis for a time-periodic transfer function in a first-order ODE, is included in *Appendix B: Derivation of the Phasor Gate Transfer Function*.

8. Proof-of-Concept Prototype

The theoretical framework and electromagnetic design principles for the Phasor Gate are now sufficiently developed to proceed with the construction and testing of a proof-of-concept prototype. This prototype will aim to demonstrate:

- Selective excitation of distinct Poloidal and Toroidal resonant modes.
- Dynamic tuning of these modes using varactors.
- Coherent frequency component mixing and phase shifting as predicted by the unitary transformation model.

A detailed plan for the prototype design, fabrication, and testing is included in *Appendix C: Proof-of-Concept Construction and Testing Plan*.

Bill of Materials

#	item	part ID	cost/unit	units	total	link
1	Varactor ≈18 pF	ALLECIN BB910	$0.3995	20	$7.99	amazon
2	Varactor ≈120 pF	Microchip KVX2301	$6.70	20	$134.00	digikey
3	STM32 Microcontroller	STM NUCLEO-H723ZG	$30.17	1	$30.17	digikey
4	Carbonyl Iron Powder	Gongyi City Meiqi I&T Co.	$8.50/kg	1 kg	$8.50	alibaba
5	Enameled Copper Wire 25AWG	EMTEL	$0.1719/ft	157 ft	$26.99	amazon
6	Single Custom PCB Order	PCBWay	$7.25/in^2	4 in^2	$29.00	pcbway
7	Op Amp 300 MHz rating	AD055ANZ	$3.15	10	$31.50	mouser
8	Resin 3D Printer & Resin	≈0.05 mm tolerance	N/A	N/A	N/A	calpoly
					Total:	$268.15

9. Harmonic Computing and Advanced Analog Processing

The successful demonstration of the Phasor Gate will be a seminal step towards two revolutionary application areas:

a) Harmonic Computing: This technology enables a new computing paradigm beyond classical and quantum approaches.

- **Qunits:** Information is encoded in the stable amplitudes and phases of multiple superposed frequencies within a single signal path, forming "qunits." These qunits can inherently represent many more states than a binary qubit (e.g., M frequencies could represent M basis states or be combined into 2^M-like dimensional spaces).
- **Rapid Computation:** Complex operations are performed via analog wave interference and resonance, potentially offering speed advantages for specific algorithms by leveraging the parallelism inherent in wave dynamics.
- **Direct Measurement:** The amplitudes and phases of the frequency components comprising a qunit are classical, continuous variables that can be measured directly using standard RF/microwave techniques, bypassing the quantum measurement problem and decoherence limitations of many qubit systems.

b) Next-Generation Analog Signal Processing: A network of Phasor Gates can form the backbone of advanced analog signal processing systems.

- **Real-Time Operation:** Being an analog device, processing occurs at the speed of signal propagation, enabling true real-time analysis and manipulation of complex waveforms.
- **Ultra-Low Power:** Operations are based on resonant energy transfer rather than power-hungry digital switching, promising significant power savings for sensing, communication, and control systems.
- **Applications:** Envisioned uses include adaptive filters with unprecedented precision, cognitive radio, dynamic spectrum management, biomedical sensor processing, and highly agile control systems for robotics and aerospace.

10. References and Literature Review

The principles underlying the Phasor Gate draw inspiration from and aim to extend several key areas of research in electromagnetism, photonics, and nonlinear dynamics. While the proposed bimodal transformer architecture and its application to Harmonic Computing represent a novel approach, they build upon established concepts and address similar goals pursued through different means. The following references provide context for these efforts.

Novel Electromagnetic Field Geometries and Topological Light: The exploration of electromagnetic fields beyond simple plane waves, focusing on their geometric and topological properties, is a vibrant research area. Rañada's foundational work presented a topological theory where electromagnetic field lines could form complex linked and knotted structures. More recently, comprehensive reviews like Arrayás, Bouwmeester, and Trueba (2017) have detailed the rich physics of knots in electromagnetism. Building on these ideas, Irvine and Bouwmeester (2008) analyzed specific knotted light solutions based on Hopf fibrations, connecting them to Chandrasekhar-Kendall states and discussing their properties and potential generation. Experimental and theoretical efforts to actively "tie knots in light fields," such as those by Kedia et al. (2013), demonstrate the increasing control over complex optical field topologies. The bimodal transformer, with its counter-wound chiral knot wires, aims to harness such geometric principles within a resonant circuit to define and manipulate distinct electromagnetic field modes, differing from free-space beam shaping but sharing the spirit of exploiting field structure.

Frequency Manipulation and Resonant Systems: The Phasor Gate's core function of controlled frequency component transformation is deeply connected to objectives in RF/microwave engineering and photonics. The precise design and analysis of resonant structures, coupling mechanisms, and wave propagation are fundamental to microwave engineering, as detailed in texts like Pozar (2005). In photonics, achieving efficient coupling of energy between elements, such as between microresonators and dielectric waveguides as analyzed by Yariv (2000), is critical for building complex systems; this principle is analogous to how we might couple energy into and out of the distinct Poloidal and Toroidal modes of the Phasor Gate, especially via dedicated windings. While existing methods for frequency conversion and shifting in both photonics (e.g., nonlinear optics, electro-optic modulators) and RF (e.g., mixers, phase-locked loops) are well-established, the Phasor Gate proposes a novel analog approach based on the parametric modulation of coupled electromagnetic field modes to achieve arbitrary unitary transformations on frequency superpositions directly.

Integrable Systems and Soliton Dynamics: The conceptual underpinnings for robust wave-based information processing find parallels in the study of integrable systems and soliton theory. Solitons, as stable solutions to certain nonlinear partial differential equations (e.g., KdV, sine-Gordon), maintain their identity through interactions, primarily experiencing phase shifts. This preservation of characteristics is highly desirable for information-carrying entities. The inverse scattering method, often described as a "nonlinear Fourier transform," allows complex nonlinear dynamics to be understood in terms of these simpler soliton components and their interactions. This deep link between wave behavior and spectral information is central to the Phasor Gate's operation. Furthermore, the rich connections between soliton theory and differential geometry, including methods like Bäcklund and Darboux transformations for generating complex solutions, inspire the exploration of "exotic" electromagnetic geometries like our bimodal transformer to achieve new functionalities. The stability and coherent interaction of solitons offer a conceptual parallel to the "qunits" envisioned for Harmonic Computing.

This brief review situates the Phasor Gate within established yet evolving research landscapes. We believe its unique approach offers a promising new avenue for both fundamental understanding and practical application.

11. Dymanet

The Phasor Gate concept stands at the confluence of novel electromagnetic theory and profound computational possibilities. Initial funding through the CIE and Noyce School of Applied Computing at Cal Poly will enable the critical first step: building and validating a prototype that demonstrates the core principles of this transformative technology. We are confident that this research will not only lead to significant academic and scientific contributions but also pave the way for groundbreaking commercial applications. We envision a world where information and energy flows harmoniously from input to output, person to person, and person to the natural world. We invite you to partner with us in bringing this vision to reality.

Help me start Dymanet – the world's first harmonic computing company.

References

[1] Rañada, A. F. (1989). A Topological Theory of the Electromagnetic Field. *Letters in Mathematical Physics, 18*(2), 97–106.

[2] Arrayás, M., Bouwmeester, D., & Trueba, J. L. (2017). Knots in electromagnetism. *Physics Reports, 667*, 1–61.

[3] Kedia, H., Bialynicki-Birula, I., Peralta-Salas, D., & Irvine, W. T. M. (2013). Tying knots in light fields. *Physical Review Letters, 111*(15), 150404.

[4] Pozar, D. M. (2005). *Microwave Engineering* (3rd ed.). Wiley.

[5] Yariv, A. (2000). Universal relations for coupling of optical power between microresonators and dielectric waveguides. *Electronics Letters, 36*(4), 321–322.

[6] Irvine, W. T. M., & Bouwmeester, D. (2008). Linked and knotted beams of light. *Nature Physics, 4*(9), 716–720.

[7] Gu, C. (Ed.). (1995). *Soliton Theory and Its Applications*. Springer-Verlag.

Appendix A: Bimodal Transformer Parameterization Images

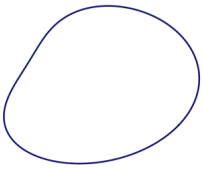

(1, 1) Knot

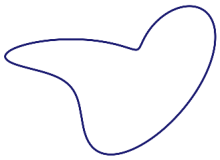

(2, 1) Knot

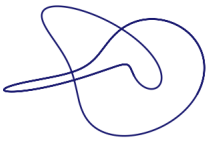

(3, 2) Knot

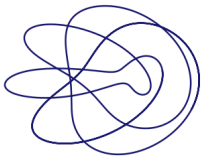

(5, 4) Knot

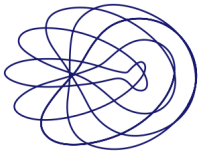

(7, 6) Knot

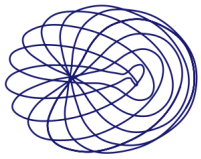

(10, 9) Knot

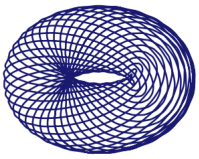

(25, 24) Knot

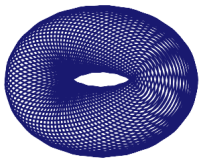

(50, 49) Knot

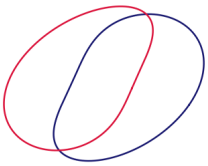

(1, 1) 2-Knot

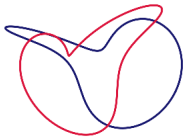

(2, 1) 2-Knot

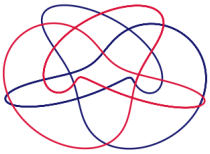

(3, 2) 2-Knot

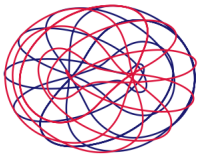

(7, 6) 2-Knot

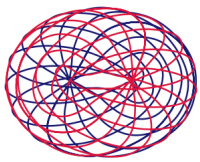

(10, 9) 2-Knot

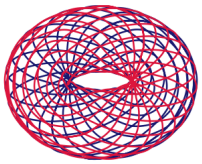

(15, 14) 2-Knot

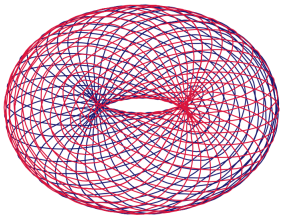

(25, 24) 2-Knot

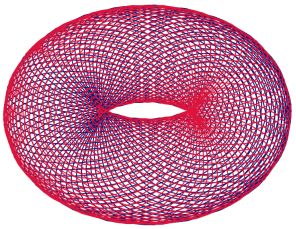

(50, 49) 2-Knot

Appendix B: Derivation of the Phasor Gate Transfer Function

This appendix outlines the derivation of the 2×2 unitary matrix $P(\Theta, \tau)$ that describes the transformation of an input signal state in the Poloidal (P) mode to an output signal state in the Toroidal (T) mode of the Phasor Gate. The derivation relies on solving the coupled mode equations for the signal envelopes under parametric modulation.

B.1. Defining the Modes and Resonances

Start by defining the Poloidal (x_P) and Toroidal (x_T) mode amplitudes as the quantities that oscillate. Both x_P and x_T are voltage waveform frequency superpositions. Their uncoupled equations would be simple harmonic oscillators.

$$\ddot{x}_P(t) + \omega_{P0}^2 x_P(t) = 0$$

$$\ddot{x}_T(t) + \omega_{T0}^2 x_T(t) = 0$$

We replace ω_{P0} and ω_{T0} with parametrically modulated resonant angular frequencies, arising from the varactor networks.

$$\Omega_P(t) = \omega_c + \Delta\Omega_P \sin(\omega_m t)$$

$$\Omega_T(t, \Theta) = \omega_c + \Delta\Omega_T \sin(\omega_m t + \Theta)$$

where $\omega_c = \pi(f_1 + f_2)$, $\Delta\Omega_P$ and $\Delta\Omega_T$ are amplitudes of frequency deviation (e.g., $\pi|f_1 - f_2|$), and $\omega_m = 2\pi|f_1 - f_2|$. The oscillator equations become (neglecting damping for unitary evolution):

$$\ddot{x}_P(t) + \Omega_P^2(t) x_P(t) + K x_T(t) = F_{inP}(t) \quad \text{(Input to Poloidal mode)}$$

$$\ddot{x}_T(t) + \Omega_T^2(t) x_T(t) + K x_P(t) = 0 \quad \text{(Output from Toroidal mode)}$$

Here K represents the physical coupling strength between the P and T modes (e.g., from the shared geometry of the bimodal transformer itself, before considering varactor-induced couplings for $f_1 \leftrightarrow f_2$ mixing within each mode via $\Omega(t)$). The term $F_{inP}(t)$ represents the forcing of the Poloidal mode by the input voltage superposition $V_i = a\sin(\omega_1 t + \phi_1) + b\sin(\omega_2 t + \phi_2)$.

B.2. Transition to Slowly Varying Envelopes

We seek solutions near frequencies ω_1 and ω_2. We can express $x_P(t)$ and $x_T(t)$ using slowly varying complex envelopes $P_1(t), P_2(t), T_1(t), T_2(t)$:

$$x_P(t) = \text{Re}\{P_1(t)e^{j\omega_1 t} + P_2(t)e^{j\omega_2 t}\}$$

$$x_T(t) = \text{Re}\{T_1(t)e^{j\omega_1 t} + T_2(t)e^{j\omega_2 t}\}$$

(In Floquet analysis it is often standard to scale by $1/\sqrt{2\omega_c}$, but this can be omitted – under the SVA approximation, input sine waves become *complex numbers*). Apply the Slowly Varying Envelope Approximation (SVEA): $\dot{P}_k$ is small, $\ddot{P}_k \approx 0$. So, $\ddot{x}_P(t) \approx \text{Re}\{-\omega_1^2 P_1 e^{j\omega_1 t} + 2j\omega_1 \dot{P}_1 e^{j\omega_1 t} - \omega_2^2 P_2 e^{j\omega_2 t} + 2j\omega_2 \dot{P}_2 e^{j\omega_2 t}\}$.

B.3. Applying the Rotating Wave Approximation (RWA)

For the parametric terms, expand $\Omega_k^2(t) \approx \omega_c^2 + 2\omega_c \Delta\Omega_k \sin(\omega_{k_m} t + \text{phase}_k)$. Substitute the envelope forms into the coupled ODEs. For each equation (e.g., for x_P), collect terms oscillating at $e^{j\omega_1 t}$ and $e^{j\omega_2 t}$ separately. This is important: The term $2\omega_c \Delta\Omega_P \sin(\omega_m t) x_P(t)$ will contain products like $\sin(\omega_m t) P_2(t) e^{j\omega_2 t}$. Since $\omega_m = \omega_1 - \omega_2$ (assuming $\omega_1 > \omega_2$),

$$\sin(\omega_m t) P_2(t) e^{j\omega_2 t} = \frac{e^{j\omega_m t} - e^{-j\omega_m t}}{2j} P_2(t) e^{j\omega_2 t}$$

The term $e^{j\omega_m t} e^{j\omega_2 t} = e^{j\omega_1 t}$ is resonant for the $\dot{P}_1$ equation. The term $e^{-j\omega_m t} e^{j\omega_2 t} = e^{j(2\omega_2 - \omega_1)t}$ is non-resonant under RWA if $2\omega_2 - \omega_1$ is far from ω_1, ω_2. This leads to terms like $(2\omega_c \Delta\Omega_P)\frac{1}{2j} P_2$ contributing to the $\dot{P}_1$ equation. This also means the phasor gate is much more robust when processing adjacent harmonics well above the first harmonic (ω_m).

B.4. First-Order Coupled Equations for Envelopes

After applying SVEA and RWA, and collecting terms for each envelope, you will arrive at a system of first-order ODEs. For example, the equation for $\dot{P}_1$ will look schematically like:

$$2j\omega_1 \dot{P}_1 + (\omega_c^2 - \omega_1^2) P_1 \approx (\text{coeff}) P_2 + K T_1 + F_{in,1}$$

The term $(\omega_c^2 - \omega_1^2) P_1$ represents a detuning from a central frequency. In an appropriately chosen rotating frame (or if ω_c is defined as the average of ω_1 and ω_2 and these are the mode's natural frequencies in that frame), these detuning terms can be set to zero, simplifying the diagonal of $\mathbf{H}_{\text{eff}}$. The system takes the form $\frac{d}{dt}\mathbf{A} = -i\mathbf{H}_{\text{eff}}(\Theta)\mathbf{A} + \mathbf{F}'_{in}$. Now, explicitly define the elements of $\mathbf{H}_{\text{eff}}(\Theta)$ based on the geometries of interaction in the structure: * $H_{P_1P_2} (= G_P^*$ or $i\mathcal{G}_P)$ comes from $2\omega_c \Delta\Omega_P \sin(\omega_m t)$ term coupling $P_2 \to P_1$. * $H_{T_1T_2} (= G_T^*$ or $i\mathcal{G}_{T0} e^{j\Theta})$ comes from $2\omega_c \Delta\Omega_T \sin(\omega_m t + \Theta)$ term coupling $T_2 \to T_1$. * $H_{P_1T_1} (= \kappa')$ comes from $K/(2\omega_1)$, etc. If the modulation drive is $\sin(\omega_m t)$, the resulting coupling term in $\mathbf{H}_{\text{eff}}$ is imaginary (a σ_y-like drive). If it were $\cos(\omega_m t)$, it would be real (a σ_x-like drive). Based on $\Omega_P(t) = \ldots \sin(\omega_m t)$ and $\Omega_T(t) = \ldots \sin(\omega_m t + \Theta)$, the Hamiltonian should be (assuming $\mathcal{G}_P, \mathcal{G}_{T0}, \kappa'$ are real strengths):

$$\mathbf{H}_{\text{eff}}(\Theta) = \begin{pmatrix} 0 & i\mathcal{G}_P & \kappa' & 0 \\ -i\mathcal{G}_P & 0 & 0 & \kappa' \\ \kappa' & 0 & 0 & i\mathcal{G}_{T0} e^{-j\Theta} \\ 0 & \kappa' & -i\mathcal{G}_{T0} e^{j\Theta} & 0 \end{pmatrix}$$

Again, the state of the signal in the P-mode is now represented by the complex amplitudes $(P_1(t), P_2(t))$ for frequencies ω_1, ω_2, and similarly $(T_1(t), T_2(t))$ for the T-mode. Based on the parametrically modulated resonant frequencies $\Omega_P(t)$ and $\Omega_T(t, \Theta)$, and inter-mode coupling K, and applying the Slowly Varying Envelope Approximation (SVEA) and Rotating Wave Approximation (RWA) (justified by Floquet theory principles for periodic modulation at $\omega_m = |\omega_1 - \omega_2|$), the system dynamics are described by:

$$\frac{d}{dt}\mathbf{A}(t) = -i\mathbf{H}_{\text{eff}}(\Theta)\mathbf{A}(t)$$

where $\mathbf{A}(t) = (P_1(t), P_2(t), T_1(t), T_2(t))^T$.

For clarity and to illustrate the core Θ-dependent transformation, let's make the simplifying assumption that there is no direct $f_1 \leftrightarrow f_2$ mixing within the P-mode itself ($G_P = 0$). This can safely be assumed if we

are forcing a voltage onto the poloidal mode, which is very close to what we are doing (the input coil and the Poloidal mode are magnetically coupled). The effective Hamiltonian $\mathbf{H}_{\text{eff}}(\Theta)$ is then:

$$\mathbf{H}_{\text{eff}}(\Theta) = \begin{pmatrix} 0 & 0 & \kappa' & 0 \\ 0 & 0 & 0 & \kappa' \\ \kappa' & 0 & 0 & G_{T0}e^{-j\Theta} \\ 0 & \kappa' & G_{T0}e^{j\Theta} & 0 \end{pmatrix}$$

Here:

- κ' is the real coupling strength between P-mode and T-mode components at the same frequency (e.g., $P_1 \leftrightarrow T_1$), derived from K and average frequencies ($\kappa' \approx K/(2\omega_c)$).
- G_{T0} is the real magnitude of the $f_1 \leftrightarrow f_2$ mixing strength within the T-mode, driven by the parametric modulation of $\Omega_T(t, \Theta)$ (i.e., $G_{T0} \propto \Delta\Omega_T$, where $\Delta\Omega_T = \pi|f_1 - f_2|$ is the amplitude of the resonant frequency deviation).
- Θ is the quasimodal phase, controlling the phase of the $f_1 \leftrightarrow f_2$ mixing in the T-mode.

The input state is $\mathbf{A}(0) = (A_1, A_2, 0, 0)^T$. The output T-mode state at time τ is $(T_1(\tau), T_2(\tau))^T$.

B.5. Solution via Laplace Transform

Let $\mathcal{L}\{f(t)\} = \tilde{f}(s)$. The system of ODEs becomes:

$$\begin{aligned} s\tilde{P}_1(s) - A_1 &= -i\kappa'\tilde{T}_1(s) \\ s\tilde{P}_2(s) - A_2 &= -i\kappa'\tilde{T}_2(s) \\ s\tilde{T}_1(s) &= -i\kappa'\tilde{P}_1(s) - iG_{T0}e^{-j\Theta}\tilde{T}_2(s) \\ s\tilde{T}_2(s) &= -i\kappa'\tilde{P}_2(s) - iG_{T0}e^{j\Theta}\tilde{T}_1(s) \end{aligned}$$

Substituting $\tilde{P}_1(s)$ and $\tilde{P}_2(s)$ from the first two equations into the latter two, we obtain a system for $\tilde{T}_1(s)$ and $\tilde{T}_2(s)$:

$$\begin{pmatrix} \frac{s^2+\kappa'^2}{s} & iG_{T0}e^{-j\Theta} \\ iG_{T0}e^{j\Theta} & \frac{s^2+\kappa'^2}{s} \end{pmatrix} \begin{pmatrix} \tilde{T}_1(s) \\ \tilde{T}_2(s) \end{pmatrix} = -\frac{i\kappa'}{s} \begin{pmatrix} A_1 \\ A_2 \end{pmatrix}$$

Let $X(s) = \frac{s^2+\kappa'^2}{s}$. The matrix on the left is $\begin{pmatrix} X(s) & iG_{T0}e^{-j\Theta} \\ iG_{T0}e^{j\Theta} & X(s) \end{pmatrix}$. Its determinant is $\Delta_{sys}(s) = X(s)^2 - (iG_{T0}e^{-j\Theta})(iG_{T0}e^{j\Theta}) = X(s)^2 + G_{T0}^2$. So, $\Delta_{sys}(s) = \left(\frac{s^2+\kappa'^2}{s}\right)^2 + G_{T0}^2 = \frac{(s^2+\kappa'^2)^2+s^2G_{T0}^2}{s^2}$. The inverse is $\frac{1}{\Delta_{sys}(s)} \begin{pmatrix} X(s) & -iG_{T0}e^{-j\Theta} \\ -iG_{T0}e^{j\Theta} & X(s) \end{pmatrix}$. Thus, the s-domain transformation $\mathbf{M}(s, \Theta)$ such that $\begin{pmatrix} \tilde{T}_1(s) \\ \tilde{T}_2(s) \end{pmatrix} = \mathbf{M}(s, \Theta) \begin{pmatrix} A_1 \\ A_2 \end{pmatrix}$ is:

$$\mathbf{M}(s, \Theta) = \frac{-i\kappa' s}{(s^2 + \kappa'^2)^2 + s^2G_{T0}^2} \begin{pmatrix} \frac{s^2+\kappa'^2}{s} & -iG_{T0}e^{-j\Theta} \\ iG_{T0}e^{j\Theta} & \frac{s^2+\kappa'^2}{s} \end{pmatrix}$$

Explicitly:

$$M_{11}(s) = \frac{-i\kappa'(s^2+\kappa'^2)}{(s^2+\kappa'^2)^2+s^2G_{T0}^2}$$
$$M_{12}(s,\Theta) = \frac{-i\kappa' s(-iG_{T0}e^{-j\Theta})}{(s^2+\kappa'^2)^2+s^2G_{T0}^2} = \frac{-\kappa' G_{T0}e^{-j\Theta}s}{(s^2+\kappa'^2)^2+s^2G_{T0}^2}$$
$$M_{21}(s,\Theta) = \frac{-i\kappa' s(iG_{T0}e^{j\Theta})}{(s^2+\kappa'^2)^2+s^2G_{T0}^2} = \frac{\kappa' G_{T0}e^{j\Theta}s}{(s^2+\kappa'^2)^2+s^2G_{T0}^2}$$
$$M_{22}(s) = M_{11}(s)$$

B.6. Characteristic Frequencies and Time-Domain Solution

The time-domain behavior $P(\Theta,\tau) = \mathcal{L}^{-1}\{\mathbf{M}(s,\Theta)\}(\tau)$ is determined by the poles of $\mathbf{M}(s,\Theta)$, which are the roots of the characteristic equation $D(s) = (s^2+\kappa'^2)^2 + s^2G_{T0}^2 = 0$.

$$s^4 + (2\kappa'^2 + G_{T0}^2)s^2 + \kappa'^4 = 0$$

This is a quadratic in s^2. Let $y = s^2$: $y^2 + (2\kappa'^2 + G_{T0}^2)y + \kappa'^4 = 0$. The roots for s^2 are $s^2 = \frac{-(2\kappa'^2+G_{T0}^2)\pm\sqrt{(2\kappa'^2+G_{T0}^2)^2-4\kappa'^4}}{2} = \frac{-(2\kappa'^2+G_{T0}^2)\pm G_{T0}\sqrt{4\kappa'^2+G_{T0}^2}}{2}$. Since $2\kappa'^2 + G_{T0}^2 > G_{T0}\sqrt{4\kappa'^2+G_{T0}^2}$ (as $(2\kappa'^2+G_{T0}^2)^2 = 4\kappa'^4 + 4\kappa'^2G_{T0}^2 + G_{T0}^4 > G_{T0}^2(4\kappa'^2+G_{T0}^2)$), both roots for s^2 are negative real numbers. Let $s^2 = -\omega_a^2$ and $s^2 = -\omega_b^2$, where $\omega_a^2, \omega_b^2 > 0$.

$$\omega_{a,b}^2 = \frac{(2\kappa'^2+G_{T0}^2) \mp G_{T0}\sqrt{4\kappa'^2+G_{T0}^2}}{2}$$

The four poles are $s = \pm i\omega_a, \pm i\omega_b$. These purely imaginary poles ensure that the time-domain solutions are oscillatory (linear combinations of $\cos(\omega_k\tau)$ and $\sin(\omega_k\tau)$), corresponding to unitary evolution for a lossless system.

B.7. The Unitary Transformation Matrix $P(\Theta,\tau)$

The inverse Laplace transforms of the elements $M_{ij}(s,\Theta)$ will yield the elements $P_{ij}(\Theta,\tau)$ of our desired 2×2 matrix.

- $P_{11}(\tau) = P_{22}(\tau) = \mathcal{L}^{-1}\{M_{11}(s)\}(\tau)$. Since $M_{11}(s) = \frac{-i\kappa'(s^2+\kappa'^2)}{D(s)}$, and $D(s)$ is an even function of s, $M_{11}(s)$ is an odd function of s times $-i$. Its inverse Laplace transform will be a real, even function of τ (a sum of cosines). Let $P_{11}(\tau) = \alpha(\tau)$, where $\alpha(\tau)$ is real.
- $P_{12}(\tau,\Theta) = e^{-j\Theta}\mathcal{L}^{-1}\{\frac{-\kappa' G_{T0}s}{D(s)}\}(\tau)$. The term $\frac{-\kappa' G_{T0}s}{D(s)}$ is an odd function of s. Its inverse Laplace transform will be a real, odd function of τ (a sum of sines) multiplied by $-i$ (implicitly from a standard sine transform definition or by analyzing residues). Let $\mathcal{L}^{-1}\{\frac{-\kappa' G_{T0}s}{D(s)}\}(\tau) = -i\sigma(\tau)$, where $\sigma(\tau)$ is real. Then $P_{12}(\tau,\Theta) = -i\sigma(\tau)e^{-j\Theta}$.
- $P_{21}(\tau,\Theta) = e^{j\Theta}\mathcal{L}^{-1}\{\frac{\kappa' G_{T0}s}{D(s)}\}(\tau) = i\sigma(\tau)e^{j\Theta}$.

Thus, the transformation matrix is:

$$P(\Theta,\tau) = \begin{pmatrix} \alpha(\tau) & -i\sigma(\tau)e^{-j\Theta} \\ i\sigma(\tau)e^{j\Theta} & \alpha(\tau) \end{pmatrix}$$

For this matrix to be unitary, we require $PP^\dagger = \mathbf{I}$, which implies $|\alpha(\tau)|^2 + |-i\sigma(\tau)e^{-j\Theta}|^2 = 1$, so $\alpha(\tau)^2 + \sigma(\tau)^2 = 1$. This condition will naturally be satisfied by the functions derived from the inverse Laplace transform of a system representing unitary evolution. We can therefore define an angle $\phi_0(\tau)$ such that: $\alpha(\tau) = \cos(\phi_0(\tau)/2)$ $\sigma(\tau) = \sin(\phi_0(\tau)/2)$

The matrix $P(\Theta, \tau)$ then becomes:

$$P(\Theta,\tau) = \begin{pmatrix} \cos(\phi_0(\tau)/2) & -ie^{-i\Theta}\sin(\phi_0(\tau)/2) \\ -ie^{j\Theta}\sin(\phi_0(\tau)/2) & \cos(\phi_0(\tau)/2) \end{pmatrix}$$

This matrix represents a rotation by an angle $\phi_0(\tau)$ (which is a function of τ, κ', and G_{T0} through ω_a, ω_b) around an axis $\hat{n}(\Theta) = (\cos\Theta, \sin\Theta, 0)$ in the X-Y plane of the Bloch sphere. The explicit forms of $\cos(\phi_0(\tau)/2)$ and $\sin(\phi_0(\tau)/2)$ are specific combinations of $\cos(\omega_a\tau)$, $\cos(\omega_b\tau)$, $(\sin(\omega_a\tau))/\omega_a$, and $(\sin(\omega_b\tau))/\omega_b$.

B.8. Conclusion

This derivation path, starting from the coupled mode equations and using the Laplace transform method for the simplified case ($G_P = 0$), rigorously establishes that the P-to-T transformation $P(\Theta, \tau)$ takes the form of a unitary SU(2) rotation. The quasimodal phase Θ controls the axis of this rotation in the X-Y plane, and the interaction time τ (along with system constants κ', G_{T0}) controls the angle of rotation $\phi_0(\tau)$. This provides a concrete mathematical basis for the Phasor Gate's ability to perform arbitrary unitary operations when combined with external Z-rotations, thus validating its potential for Harmonic Computing and advanced analog signal processing. A more general derivation with $G_P \neq 0$ would follow similar principles but with more complex algebra, still resulting in a 2×2 unitary $P(\Theta, \tau)$ whose elements depend on all parameters.

Appendix C: Proof-of-Concept Construction and Testing Plan

C.1 Introduction and Timeline Overview

This appendix details the methodology for constructing and testing a proof-of-concept (PoC) Phasor Gate. The objective is to experimentally validate the theoretical framework outlined in Section 7 and Appendix B, demonstrating controllable unitary transformations on frequency-superimposed AC signals. The construction will leverage components from the Bill of Materials (Section 8, Page 4) and facilities available at Cal Poly. We are driven by the conviction that this prototype will provide compelling evidence for the transformative potential of Harmonic Computing and advanced analog processing.

Estimated Summer Timeline:

- **Weeks 1-2 (June 2025):** Detailed electromagnetic (EM) simulation of the bimodal transformer geometry (using parameters like $R_P = 4$ cm, $R_T = 2$ cm, $N = 30$ turns for (30,29)-knots). Finalize varactor network design, component selection, and PCB layout. Refine STM32 control signal strategy for varactor biasing and modulation.
- **Weeks 3-4 (June - July 2025):** Fabrication of 3D-printed toroidal formers. Procurement of all electronic components (varactors, STM32, op-amps, passives, carbonyl iron powder, enameled wire). PCB fabrication order.
- **Weeks 5-6 (July 2025):** Assembly of the bimodal transformer core, including chiral wire winding and integration of magnetic material. Assembly of the control and measurement PCB.
- **Weeks 7-8 (July - August 2025):** Sub-system testing: varactor capacitance vs. voltage characterization, I/O coil impedance measurements, STM32 signal generation (DC biases, AC modulation waveforms, input f_1, f_2 test signals), op-amp circuit verification.
- **Weeks 9-10 (August 2025):** Full system integration. Initial testing: DC response, static frequency response of the unmodulated gate. Characterization of Poloidal and Toroidal mode resonant frequencies and Q-factors across the varactor tuning range.
- **Months 3-5 (August 2025 - October 2025):** Dynamic testing: Implement parametric modulation. Experimentally measure the transfer function $P(\Theta, \tau)$ for steps of $\Theta = \pi/4$ and varying τ. Validate against the analytically derived transfer function. Test ϕ_0 control via trapezoidal waveform shaping.
- **Month 5+ (From October 2025):** Iterate on prototype design for Q-factor enhancement and optimized mode coupling. Begin exploration of networked Phasor Gates, investigate CNOT gate implementation, and design experiments to demonstrate analog qunit superposition. Initiate research into miniaturization and integrated chip-scale designs.

C.2 Detailed Prototype Construction Methodology

C.2.1 Bimodal Transformer Core Fabrication (Single Torus Design)

The heart of the Phasor Gate is the bimodal transformer. Our primary PoC approach focuses on the single-torus design depicted in Section 1 (Page 1) and underpinning the derived $\mathbf{H}_{\text{eff}}$.

1. **Toroidal Former Design:** A toroidal former with nominal dimensions (e.g., Poloidal radius $R_P = 4$ cm, Toroidal radius $R_T = 2$ cm) will be designed using CAD software. Crucially, this former will incorporate two distinct sets of precisely defined, counter-rotating helical grooves corresponding to (N, N-1) toroidal knots (e.g., N=30 turns for (30,29)-knots). These grooves will guide the two chiral windings. The torus will be designed to be hollow.

2. **3D Printing:** The former will be fabricated in multiple pieces using a high-resolution resin 3D printer (e.g., ≈ 0.05 mm tolerance, utilizing Cal Poly facilities). The design will allow for assembly into a complete torus. Specifically, the torus will be conceptually "sliced" (e.g., two halves, plus a removable section or lid) to allow access to its hollow interior.

3. **Magnetic Core Material Integration:** After initial assembly of the main toroidal structure (leaving an opening), the hollow interior will be carefully filled with Carbonyl Iron Powder. This material is chosen for its suitable RF magnetic properties to concentrate the fields and potentially enhance inductance. The powder may be mixed with a non-conductive epoxy binder for stability, or packed carefully.

4. **Final Assembly:** Once filled, the remaining 3D-printed pieces (e.g., the ring section sliced from the top to expose the hollow inside) will be securely glued or fastened to complete the toroidal core.

C.2.2 Chiral and Input/Output Winding Implementation

1. **Chiral Windings:** Two continuous lengths of 25 AWG enameled copper wire will be meticulously wound into the pre-designed grooves on the assembled toroidal core. One wire will follow the left-handed (N,N-1) knot path, and the other will follow the right-handed (N,N-1) knot path, creating the interleaved bimodal structure. Consistent tension will be maintained. The N=30 turns will provide sufficient inductance and mode interaction. The four ends of these two wires (two per wire) will be carefully prepared for connection to the varactor network.

2. **Input Coil (Poloidal Drive):** A separate coil will be wound toroidally around the major circumference of the bimodal transformer core (potentially around an integrated bobbin or directly over the primary chiral windings if shielded). This coil, when driven with an AC current, will primarily generate a Poloidal magnetic field (B_P) to excite the P-mode of the bimodal core. It will consist of approximately 30 turns of enameled copper wire.

3. **Output Coil (Toroidal Sense):** Another separate coil will be wound poloidally around the minor circumference of the bimodal transformer core (like a solenoidal winding segment). This coil will primarily sense the Toroidal magnetic field (B_T) generated by the T-mode of the bimodal core. It will also consist of approximately 30 turns.

4. **Electrical Isolation:** The input and output coils will be electrically isolated from the bimodal transformer's chiral windings and varactor network, ensuring coupling is purely magnetic. Magnetic shielding (using ferrite or other RF magnetic materials, possibly incorporating the carbonyl iron powder more strategically) between the P and T mode regions within the core and around the I/O coils will be explored to enhance mode purity, as per the "magnetic shells" concept.

Alternative constructions

Two-Torus: Should the single-torus interleaved winding prove initially too complex for fabrication, an alternative involves two separate 3D-printed tori – one with left-handed grooves, the other with right-handed. Each chiral wire is wound on its respective torus. The tori are then mechanically linked (e.g., one passing through the center of the other). The varactor network then bridges the ends of the wire on the first torus to the ends of the wire on the second. The input coil would be wound on one torus, the output on the other. While not identical to the primary theoretical model, this could allow for testing the varactor control and P-T mode concepts with a different coupling topology.

Galinstan: Wires can be formed from negative channels in a precision 3D print. Using negative pressure, a liquid conductor can be pumped through all windings, providing a liquid wire to form the inductive elements of the system. While more costly, this would simplify the design, fabrication, and winding process tremendously.

C.2.3 Varactor Network Design and Assembly

Two independent varactor networks will couple the two chiral windings. One network will primarily influence the Poloidal mode resonances ("Poloidal capacitors"), and the other the Toroidal mode resonances ("Toroidal capacitors").

1. **Capacitance Range and Resolution:** Each network aims for a dynamically controllable capacitance from approximately 100 pF to 2000 pF. To achieve this range with fine resolution, we will employ a parallel arrangement of multiple varactors.

2. **"Tens/Ones Place" Control:** We will use larger capacitance varactors (e.g., Microchip KVX2301, ≈ 120 pF nominal, from the Bill of Materials) for coarse, "tens-place" adjustment, and smaller capacitance varactors (e.g., BB910, ≈ 18 pF nominal) for fine, "ones-place" adjustment. Approximately 5-10 varactors of each type might be used per network, wired in parallel.

3. **STM32 Control Signal Delivery:** The STM32 microcontroller will generate separate DC bias voltages for each varactor (or small groups of them if ganged for the binary counter system). These DC biases will be summed with the AC modulation signal ($f_m = |f_1 - f_2|$ with phase Θ) also generated by the STM32 (via DAC or filtered PWM) and scaled by op-amps. Each of the four conceptual varactors (connecting each red wire end to each blue wire end) will thus be realized by one of these parallel banks, with two banks forming the Poloidal network and two forming the Toroidal network, each independently controlled.

4. **Mounting:** Both surface-mount (BB910) and through-hole (KVX2301 if a through-hole variant is sourced, or SMD equivalent) varactors will be mounted on the custom PCB, along with their biasing resistors and RF isolation chokes.

C.2.4 Control and Measurement Circuitry

1. **Signal Generation (Input V_i):** The STM32 microcontroller will digitally synthesize the input waveform $V_i = a\sin(2\pi f_1 t + \phi_1) + b\sin(2\pi f_2 t + \phi_2)$. Its DAC output will be appropriately filtered and then scaled/buffered using an op-amp (e.g., AD055ANZ) to drive the Poloidal input coil.

2. **Modulation Signal Generation:** The STM32 will also generate the f_m sinusoidal (or trapezoidal) modulation signals for the varactor networks, including the crucial quasimodal phase offset Θ between the signals for the Poloidal and Toroidal varactor sets.

3. **Output Measurement (V_o):** The voltage output from the Toroidal sense coil will be captured. This can be done in two ways:

   - Directly using a high-bandwidth oscilloscope for initial characterization and visualization.
   - For automated measurement and data logging, the signal can be appropriately scaled, filtered, and then digitized using either an external ADC or a built-in ADC/digital codec interface on the STM32 (if performance is adequate for the frequencies f_1, f_2). Digital signal processing (e.g., FFT) on the STM32 or a connected computer will then extract the amplitudes and phases of the f_1, f_2 components.

C.3 Experimental Testing and Validation Plan

A phased approach will be used for testing:

1. **Component and Sub-System Characterization (Weeks 7-8):**

   - Individual varactor $C - V$ curves measured to confirm tuning range and select matched sets.
   - Frequency response of the control signal paths (STM32 DAC/PWM $\rightarrow$ op-amp $\rightarrow$ varactor bias input).
   - Impedance vs. frequency measurement of the wound chiral coils and I/O coils (inductance, self-resonant frequency).

2. **Static and Dynamic Response of Assembled Gate (Weeks 9-10):**

   - *DC Response:* Not directly applicable for AC resonances, but check for shorts/opens.
   - *Static Resonances:* With varactors set to fixed DC biases (no AC modulation), sweep input frequency and measure transmission from input Poloidal coil to output Toroidal coil to identify the resonant frequencies of the P and T modes. Map these resonant frequencies and their Q-factors across the full DC tuning range of the varactor networks. This validates basic mode excitation and tunability.

3. **Verification of Unitary Transformation Control (Months 3-5):**

   - Apply the input signal V_i (superposition of f_1, f_2) to the Poloidal input coil.
   - Activate the parametric modulation on the varactor networks at $f_m = |f_1 - f_2|$.
   - Measure the output V_o from the Toroidal coil. Decompose it into f_1, f_2 components to determine their new amplitudes and phases (B_1, B_2).
   - Systematically vary the quasimodal phase Θ in steps (e.g., $\pi/4$) while keeping interaction time τ (and other parameters like $\Delta\Omega_T, K$ effectively constant by fixing modulation amplitudes and physical setup) and reconstruct the experimental $P(\Theta)$ matrix. Compare this with the analytically derived $P(\Theta, \tau)$ from Appendix B.
   - Test the control of the effective rotation angle ϕ_0 by varying the shape of the f_m modulation waveform (trapezoidal, from near-square to near-triangle) applied to the varactors, for several fixed values of Θ. Plot the resulting transfer functions (e.g., magnitude of B_1/A_1, B_2/A_1, etc.) to quantify the change in transformation strength.

C.4 Future Development and Vision (Beyond Month 5)

The successful PoC will pave the way for more advanced development:

1. **Iterative Design for Performance Enhancement:** Build multiple copies, systematically varying design parameters (winding techniques, core materials/shells, varactor configurations) to enhance Q-factors, optimize mode coupling κ', and improve the purity of the P and T modes.

2. **Networked Phasor Gates:** Experiment with coupling multiple Phasor Gates. Investigate if a CNOT-equivalent operation (a fundamental two-qubit gate) can be realized by networking two or more Phasor Gates, where the state of one gate (e.g., presence/absence of a frequency, or its phase) controls the unitary transformation performed by another. Achieving this would satisfy key DiVincenzo criteria for a computing substrate.

3. **Analog Qunit Superposition and Entanglement Analogues:** Explore the creation of output states from networked gates that exhibit characteristics analogous to quantum superposition and entanglement – e.g., an output signal state whose frequency components cannot be described as a simple product of the states of its constituent input qunits.

4. **Miniaturization and Integration:** Investigate scaling down the Phasor Gate. Design and simulate through-hole or surface-mount components (e.g., aiming for < 1 cm^3) using advanced stereolithography or microscale 3D printing for the core, and integrated varactors/passive elements.

5. **Harmonic Computer Architecture:** Based on experimental results, begin designing chips, system architectures, and algorithms tailored for the capabilities of Harmonic Computing with qunits.

This comprehensive plan, from fundamental construction to advanced exploration, aims to rigorously establish the Phasor Gate as a viable and transformative technology. Thank you.